

# Smart Divert: A New Entry, Descent, and Landing Architecture

Michael J. Grant<sup>1</sup>, Bradley A. Steinfeldt<sup>2</sup>, and Robert D. Braun<sup>3</sup>  
*Georgia Institute of Technology, Atlanta, GA, 30332*

Gregg H. Barton<sup>4</sup>  
*Charles Stark Draper Laboratory, Houston, TX, 77058*

To date, Mars robotic landing site selection has been a compromise between scientific interest and safety. Due to the rather large landed footprint major axis lengths of the Viking, Pathfinder, Mars Exploration Rovers, and Phoenix missions, these landed ellipses have been placed in vast, relatively flat areas to ensure a high probability of landing success. Scientists are interested in exploring more geologically interesting areas that may contain landing hazards, including sloping terrain, craters, and rocks. Smart Divert is a new entry, descent, and landing architecture that could allow robotic missions to safely land in hazardous terrain without the requirement of hypersonic guidance. Smart Divert consists of a ballistic entry followed by supersonic parachute deployment. After parachute release, the vehicle diverts to one of many predefined, fuel-optimal safe zones. Smart Divert performance and entry design is discussed and is followed by a discussion of Smart Divert for random terrain. An initial assessment of optimal landing site arrangement is performed and an example of the usefulness of Smart Divert is performed for actual Mars terrain using Phoenix landing site rock count data.

## Nomenclature

$\underline{a}$	= Acceleration vector
$\underline{g}$	= Local gravity vector
$J$	= Cost function
$m_p$	= Propellant mass
$m_i$	= Initial mass of vehicle
$t_0$	= Time of divert initiation
$t_f$	= Final touchdown time
$t_{go}$	= Time-to-go
$\Gamma$	= Weighting on time-to-go
$\underline{\Delta r}$	= Position of vehicle relative to target
$\underline{\Delta v}$	= Velocity of vehicle relative to target
AGL	= Above ground level
DOF	= Degree-of-freedom
DDOR	= Delta Differential One-Way Ranging

---

<sup>1</sup> Graduate Research Assistant, Guggenheim School of Aerospace Engineering, AIAA Student Member.

<sup>2</sup> Graduate Research Assistant, Guggenheim School of Aerospace Engineering, AIAA Student Member.

<sup>3</sup> David and Andrew Lewis Associate Professor of Space Technology, Guggenheim School of Aerospace Engineering, AIAA Fellow.

<sup>4</sup> Group Leader, Mission Design Group, AIAA Senior Member.

DGB	=	Disk-gap-band
EDL	=	Entry, descent, and landing
HiRISE	=	High Resolution Imaging Science Experiment
IMU	=	Inertial measurement unit
JPL	=	Jet Propulsion Laboratory
MER	=	Mars Exploration Rovers
MRO	=	Mars Reconnaissance Orbiter
MSL	=	Mars Science Laboratory
PMF	=	Propellant mass fraction
TCM	=	Trajectory correction maneuver

## I. Introduction

TO date, entry, descent, and landing (EDL) mission designers have been forced to trade safety and scientific interest when choosing the landing site of various Mars landers. Past missions have resulted in rather large landed footprint major axis lengths ranging from 200-300 km (Viking, Pathfinder) to 80 km (Mars Exploration Rovers).<sup>1</sup> Generally, scientifically interesting landing sites are not flat and contain many landing hazards including significant variation in terrain elevation, craters, and rocks. Hence, it may be in the interest of scientists to visit these dangerous regions on Mars. However, mission designers must ensure that the majority of the landed ellipse encapsulates safe terrain. This leads the mission designers to orient the landing site ellipse over vast flat regions of Mars. It would be beneficial if science could dominate the choice of landing site location. This could be achieved with greater landed accuracy. In order to achieve improved accuracy, hypersonic guidance will be used for the first time at Mars on the Mars Science Laboratory (MSL). MSL's modified Apollo guidance algorithm utilizes only the terminal phase of the Apollo entry guidance and provides a landed footprint 20 km long in major axis through modulation of the aeroshell lift vector.<sup>2</sup> This allows MSL to travel in the vicinity of more scientifically interesting terrain. However, the implementation of hypersonic guidance increases the complexity and cost of the mission as compared to previous ballistic, unguided missions. Also, mission designers are still required to ensure the majority of the 20 km landed ellipse is over safe terrain. Smart Divert may provide a simple, low cost entry, descent, and landing architecture for landing within hazardous terrain. Smart Divert consists of a ballistic entry followed by supersonic disk-gap-band (DGB) parachute deployment at Mach 2.2, consistent with previous missions. At Mach 0.8, the parachute is released and the vehicle performs a fuel-optimal burn to a single, or one of several, safe zones identified prior to the EDL sequence. These safe zones could be identified from prior Mars orbital and surface missions much in the manner that the Mars Reconnaissance Orbiter imagery was utilized to locate a safe site for the Phoenix lander prior to this lander's arrival at Mars.

## II. Planar Example

Visualization of 3D divert trajectories is quite difficult. In order to conceptually understand Smart Divert, a simple planar example was constructed. The entry flight path angle was varied to produce a ballistic parachute deploy line (all trajectories are confined to a plane) as shown in Figure 1. Note that, in this example, the downrange spread at parachute deploy is only approximately 10 km. This may be unrealistically small and is only used to conceptually demonstrate Smart Divert. In Figure 1a, a single safe site is located at 0 km downrange. After the ballistic entry and parachute phase, each trajectory diverts to the target site on a fuel optimal trajectory. The diverts that initiate far uprange must traverse a long distance, requiring more propellant than the diverts that initiate closer to the target. In order to reduce the propellant mass fraction (PMF) required by the uprange trajectories (defined in Eq. (1) as the ratio of propellant mass to the initial mass of the vehicle), a second safe site was added uprange in the case of Figure 1b. As can be seen, the vehicle evaluates the fuel-optimal trajectory to each site and flies to the site that requires the least amount of fuel, known as the fuel optimal safe zone. In general, the uprange trajectories identify the uprange site as lowest in cost and diverted to that site. While this simple example illustrates the Smart Divert concept, the number and optimal placement of these safe zones is dependent on the size of the landing footprint and the mission-specific terrain hazards. Clearly, to implement this EDL architecture, the vehicle must also be equipped with an onboard sensor capable of enabling this safe zone decision autonomously. However, such onboard sensing and decision making is essentially equivalent to that performed by the MER DIMES system.<sup>3</sup>

$$PMF = \frac{m_p}{m_i} \quad (1)$$

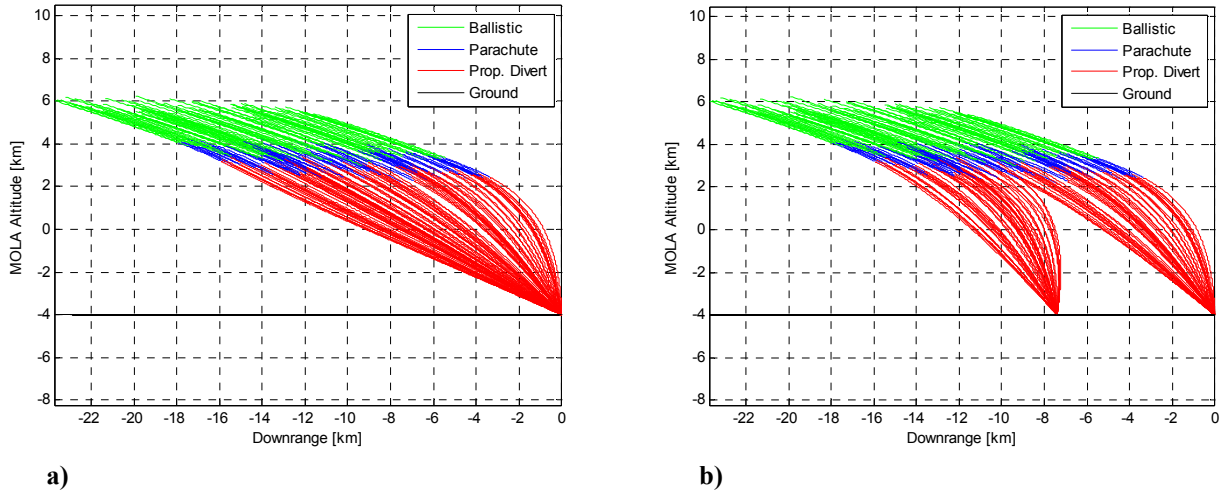


Figure 1: Example Divert to One and Two Sites

### III. Simulation Development

In order to have a flexible conceptual design tool that is capable of rapidly trading various EDL scenarios, a 3 degree-of-freedom (DOF) Mars entry simulation was developed in Matlab. The Matlab code was autocoded into a C-Mex file using the Matlab Real-Time Workshop, which reduced the execution time by an approximate factor of 35. The equations of motion were expressed in an inertial, Cartesian space. This method avoids singularities associated with angular derivatives (*e.g.*, rate of change in latitude, longitude, flight path angle, etc) as the vehicle's velocity approaches zero (*e.g.*, during terminal descent). A spherical, rotating planet with a spherical mass distribution was assumed.

In order to assess the performance of Smart Divert, a Monte Carlo environment was developed with dispersions similar to those of the MSL project.<sup>4</sup> Atmospheric properties, vehicle properties, parachute aerodynamic drag coefficient, and delivery accuracy to Mars are dispersed and are shown in Table 1 and Table 2. An MSL-class DGB parachute with a diameter of 19.5 m and drag coefficient profile shown in Figure 2 was used. Note the drag bucket near Mach 1 is captured and reduces parachute performance. This is an important consideration for low parachute deployment altitudes performed in subsequent analyses. The delivery accuracy was quantified as an entry state covariance at ten minutes prior to entry interface provided by the Jet Propulsion Laboratory (JPL) for MSL assuming the trajectory correction maneuver (TCM) 5 was performed. This covariance corresponds to state-of-the-art interplanetary navigation capability in which the vehicle is spin stabilized, delta differential one-way ranging (DDOR) is used, and a delivery error reducing TCM 5 is performed. The corresponding MSL  $3\sigma$  entry flight path angle uncertainty is approximately  $0.1^\circ$  as opposed to the Phoenix  $3\sigma$  entry flight path angle uncertainty of  $0.21^\circ$ .

Table 1: MarsGRAM 2005 Parameters

Parameter	Value / Range
Latitude [deg]	-40.60
Longitude [deg]	-62.90
Date	26 Jul 2010
Dusttau	0.1-0.9

Table 2: Monte Carlo Dispersions

Parameter	Nominal	Distribution	$3\sigma$ or min/max
Entry State	MSL Nominal	Entry Covariance	Entry Covariance
Axial Force Coefficient Multiplier	1	Gaussian	3%
Entry Mass [kg]	2196.0	Gaussian	2.0
Atmosphere Dispersion Seed	0	Uniform	1/29999
Atmosphere Update Distance [km]	0.5	Uniform	0.5/5.0
Dusttau	0.45	Uniform	0.1/0.9
Supersonic Parachute Drag	$C_D$ Profile	Uniform	-10%/+10%
Terminal Descent Engine $I_{sp}$ [sec]	194	Uniform	-0.67%/+0.67%

A set of dispersed atmospheres was generated using MarsGRAM 2005. The parameters used to generate the atmospheres are shown in Table 1. The resulting atmosphere density profiles, normalized by the nominal density profile with a Dusttau of 0.45, may be seen in Figure 3. As expected, large variations occur in the upper atmosphere. Perfect navigation throughout the EDL phase was also assumed.

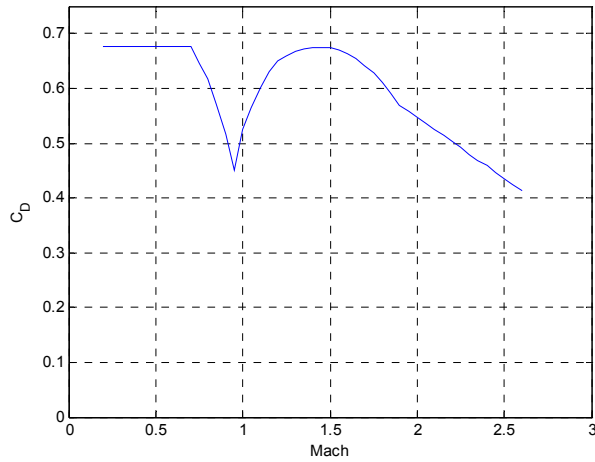


**Figure 2: Drag Coefficient vs. Mach for DGB Parachute**

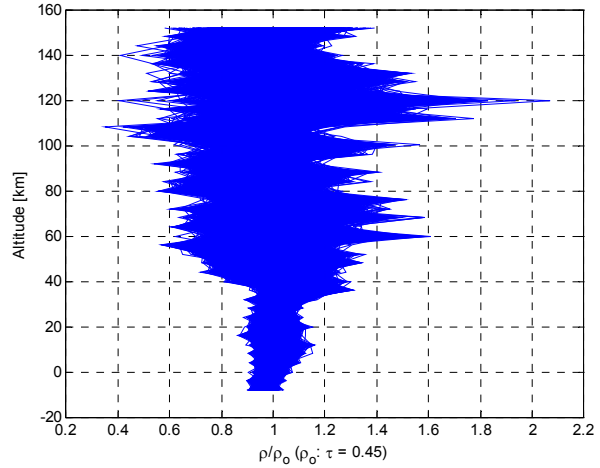


**Figure 3: Atmosphere Density Profiles**

#### IV. Simulation Validation

A Pathfinder test case was used to validate the simulation. For Pathfinder, the 585 kg vehicle entered ballistically and deployed a 12.5 m diameter supersonic disk-gap-band (DGB) parachute at a dynamic pressure of 585 Pa. At a time of 20 seconds after parachute deployment, the 64.4 kg heatshield was released. The trajectory was then propagated to the MOLA altitude immediately prior to retrorocket ignition, where the simulation was terminated. The Pathfinder entry was modeled using both the Program to Optimize Simulated Trajectories (POST) and the simulation that has been developed for this study. Figure 4 depicts both the full entry trajectory and the final phases of flight. Additionally, Table 3 compares specific trajectory event data between the two simulations. As can be seen, excellent agreement exists between these two simulations.

**Table 3: Comparison of Trajectory Event Data for Pathfinder Entry**

Event	POST	Simulation	% Difference
<b>Entry</b>			
Time (s)	0	0	0.00
Altitude (m)	128000	128000	0.00
Relative Velocity (m/s)	7479	7479	0.00
Relative Flight Path Angle (°)	-13.65	-13.65	0.00
<b>Parachute Deploy</b>			
Time (s)	154.5	154.3	-0.13
Altitude (m)	9916	9923	0.07
Relative Velocity (m/s)	414.5	415.2	0.17
Relative Flight Path Angle (°)	-23.35	-23.31	-0.17
Dynamic Pressure (Pa)	585.0	586.2	0.21
<b>Heatshield Jettison</b>			
Time (s)	174.5	174.3	-0.11
Altitude (m)	8219	8237	0.22
Relative Velocity (m/s)	90.23	90.16	-0.08
Relative Flight Path Angle (°)	-47.33	-46.56	-1.63
Dynamic Pressure (Pa)	31.98	31.88	-0.31
<b>Trajectory Termination</b>			
Time (s)	359.8	360.2	0.11
Altitude (m)	-2408	-2403	-0.21
Relative Velocity (m/s)	42.64	42.66	0.05
Relative Flight Path Angle (°)	-89.88	-88.83	-1.17
Dynamic Pressure (Pa)	21.55	21.55	0.00

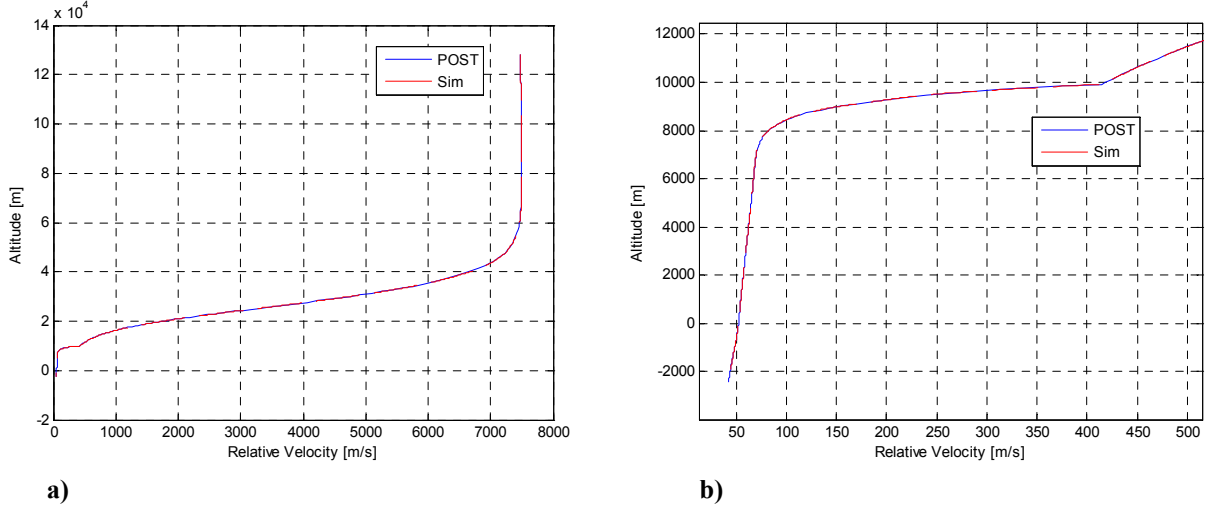


**Figure 4: Comparison of Developed Simulation and POST for Pathfinder Entry**

## V. Divert Guidance

At Mach 0.8, the parachute is released and the propulsive terminal descent phase is initiated in which the vehicle diverts from its current location to the fuel optimal safe zone. The identification of the fuel optimal safe zone could be accomplished in two ways. First, a guidance algorithm could be used along with simplified equations of motion propagated onboard the vehicle. The fuel optimal safe zone could then be chosen autonomously after evaluating the propellant required to divert to each possible safe zone. This method was employed for this analysis. Alternatively, the selection of the divert site could be pre-programmed by the ground. Due to the simplicity of ballistic entries, the relative distance traveled downrange could be inferred by the entry acceleration profile. For example, the peak deceleration loads could be used to identify where along the major axis the vehicle is likely located. From this estimated location, the vehicle could then divert to the corresponding fuel optimal safe zone identified by previous ground analysis. This approach is not likely to be fuel-optimal, but would reduce the onboard autonomy required.

A closed-form, analytic control algorithm (D'Souza guidance) has been identified as a nearly fuel-optimal terminal descent control law suitable for conceptual design.<sup>5,6</sup> The algorithm assumes a planar, non-rotating planet with negligible atmospheric forces compared to those due to gravity and thrust. The altitude is also assumed to be much smaller than the radius of the planetary body. These assumptions are quite reasonable during Mars terminal descent where the vehicle is close to the ground and traveling at subsonic speeds. In this investigation, the analytic D'Souza guidance provides the propulsive control law to perform the divert maneuver from the current time,  $t_0$ , to the final touchdown time,  $t_f$ , by minimizing the performance index shown in Eq. (2) where the weighting on time-to-go,  $\Gamma$ , is set initially to zero. The analytic control law is shown to be given by Eq (3), where the time to go,  $t_{go}$ , is the real positive root of Eq (4).  $\underline{\Delta r}$  and  $\underline{\Delta v}$  correspond to the relative position and velocity of the vehicle with respect to the target, respectively, as defined by D'Souza.<sup>6</sup>  $\underline{a}$  corresponds to the vehicle acceleration vector, and  $\underline{g}$  corresponds to the local gravity vector. The required thrust vector may then be easily obtained from the vehicle's current mass.

$$J = \Gamma t_f + \frac{1}{2} \int_{t_0}^{t_f} (\underline{a}^T \underline{a}) d\tau \quad (2)$$

$$\underline{a} = \frac{-4\underline{\Delta v}}{t_{go}} - \frac{6\underline{\Delta r}}{t_{go}^2} - \underline{g} \quad (3)$$

$$\left( \Gamma - \frac{\underline{g}^2}{2} \right) t_{go}^4 - (2\underline{\Delta v}^T \underline{\Delta v}) t_{go}^2 - (12\underline{\Delta v}^T \underline{\Delta r}) t_{go} - 18\underline{\Delta r}^T \underline{\Delta r} = 0 \quad (4)$$

Immediately prior to initiating the divert, the vehicle evaluates the fuel optimality of each safe zone by propagating simplified equations of motion using the D’Souza guidance. A complicating factor is that certain fuel optimal trajectories travel through the surface of the planet. If this occurs during the evaluation of a trajectory to a specified safe zone,  $\Gamma$  is increased until a feasible trajectory that remains above the surface is found. An increase in  $\Gamma$  results in an increase weighting on the final time, resulting in more direct trajectories that remain above the surface at the penalty of increased fuel consumption.

The analytic nature of the control law is computationally inexpensive (relative to other guidance algorithms), allows for rapid execution of Monte Carlos, and would offer similar computational advantages if used inflight. Consistent with historical Mars robotic monopropellant hydrazine terminal descent systems, a maximum thrust to weight ratio of 3 was used for the propulsive terminal descent.<sup>7</sup> Consequently, the thrust magnitude was limited if the analytic D’Souza algorithm commanded more thrust than permitted by the thrust-to-weight constraint. Using the D’Souza guidance algorithm and perfect EDL navigation, the miss distance of the vehicle at touchdown to the target is approximately 5 m. Thus, the safe zones used in this analysis resemble a single point. If implemented in an actual mission, the landed accuracy of the vehicle and, consequently, the minimum required size of the safe zones would be governed by the navigation error.

## VI. Conceptual Understanding of Smart Divert Performance

For dispersed trajectories, the flight path angle, altitude, and divert distance will vary. However, it is important to gain an understanding of the reasonable bounds of Smart Divert. As can be seen in the Smart Divert example in Figure 1, the vehicle retains a large amount of horizontal velocity at the Mach 0.8 parachute release event. Consequently, safe zones should, in general, be located downrange of the parachute deploy location to reduce the overall required propellant by accounting for the natural motion of the vehicle. This downrange bias in divert sites is discussed in the following sections. For any given dispersed trajectory, the fuel-optimal safe zone may be located along or against the natural direction of motion of the vehicle. As an average for this sensitivity analysis, the vehicle is assumed to be traveling vertically downward at Mach 0.8 (velocity of the vehicle at parachute jettison). The altitude above the ground in which the divert is initiated was varied from 4-12 km and the horizontal distance of the divert was varied from 0-50 km. Assuming the nominal MSL Isp of 194 sec, the resulting PMF for the various combinations of divert initiation altitudes and horizontal divert distances may be seen in Figure 5. The white region corresponding to the altitude of divert initiation between 4-12 km indicates divert trajectories that require a thrust-to-weight ratio larger than 3 or have in-flight Mach numbers larger than 0.8. Such cases are considered infeasible when performing a propulsive divert in a landing configuration. As expected, an increase in horizontal divert distance requires a higher divert initiation altitude. This ratio provides an effective glide slope of 3:1 for the divert. It is also important to note that initiating the divert at a higher altitude slightly increases the required PMF for the same horizontal divert distance due to increased gravity loss while thrusting. Thus, the vehicle should initiate the divert at as low of an altitude as possible for the divert distance required.

In order to feasibly implement Smart Divert as a new EDL architecture, the propellant required to perform the required divers must be maintained at a reasonable level. Previous EDL missions that propulsively landed on the surface of Mars typically employed a variation of a gravity turn control law. The PMF required to perform a gravity turn for our baseline mission is approximately 0.15. This is consistent with the 4 km altitude divert of 0 km. Figure 5 demonstrates that the mission plan should not require a divert more than 10 km to maintain a PMF less than 0.3. Figure 5 also shows that the vehicle should start the divert around 5 km above ground level (AGL) to divert a maximum of 10 km. This allows sufficient timeline to perform the divert and other final EDL events.

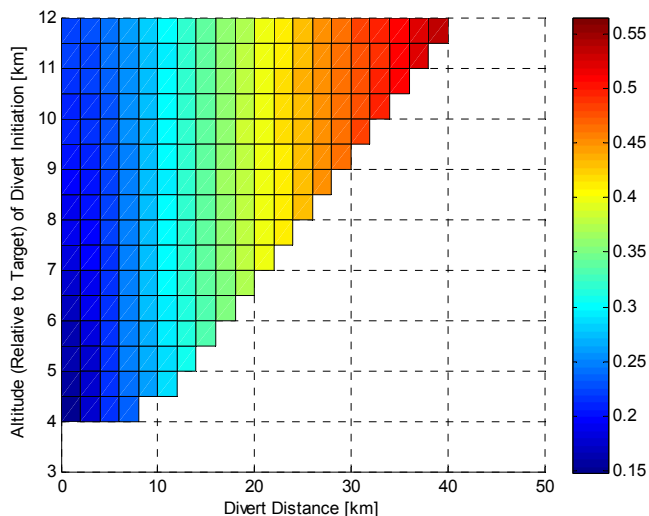
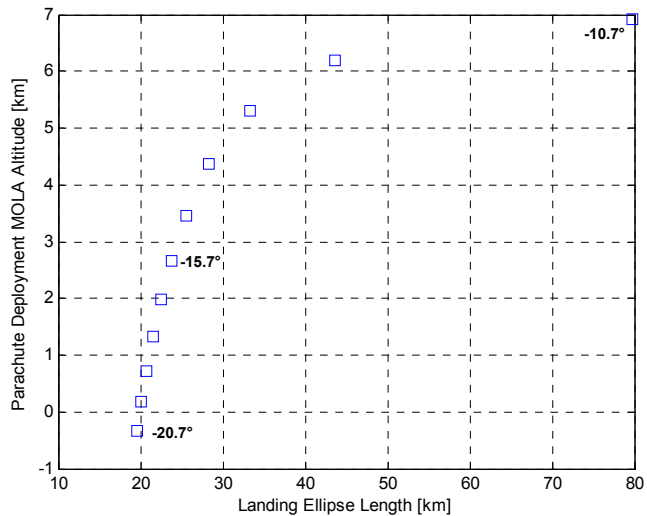


Figure 5: Propellant Mass Fraction for Various Divers

## VII. Entry Design

The entry covariance used in this investigation corresponds to the MSL mission with TCM 5 performed. The nominal relative entry flight path angle is  $-15.7^\circ$  for this covariance. Since MSL is a lifting entry, such a steep entry flight path angle results in a relatively high parachute deploy altitude relative to that of a ballistic entry due to the lifting body “pulling” the trajectory upward. The ballistic Smart Divert entry will not result in such high parachute deploy altitudes for steep entries. In order to increase altitude for ballistic entries, the entry flight path angle must be shallowed. Figure 6 shows the impact of the nominal entry flight path angle on parachute deploy MOLA altitude and landing ellipse length where each box represents a  $1^\circ$  change in EFPA from the nominal MSL value of  $-15.7^\circ$ . As expected, the parachute deploy altitude decreases as the entry flight path angle is steepened. It is assumed that the navigation and delivery errors remain unchanged across the EFPA range considered. Hence, the influence of the error in entry flight path angle on the landed ellipse length increases as the entry flight path angle is shallowed. This is extremely important for mission design. A shallower entry flight path angle permits high parachute deploy altitudes at the cost of an increase in landed ellipse length. Thus, in order to perform Smart Divert at high elevations, the corresponding landing ellipse length may be quite large. For the shallowest entry near  $-11^\circ$ , the corresponding landing ellipse length is approximately 80 km, consistent with MER. Consequently, a great number of safe zones will have to be identified for high altitude parachute deploy conditions to ensure the required PMF remains reasonable. While dependent on vehicle ballistic coefficient, in order to provide a 5 km spread between terminal descent initiation and the ground, it is unlikely that landing site elevations greater than 2 km MOLA will be chosen for Smart Divert unless a large number of safe zones can be identified. Note that mission design alternatives exist to increase the parachute deploy altitude relative to that assumed in this investigation, including the use of hypersonic guidance, the use of unguided full lift-up entries, and the use of inflatable aerodynamic decelerators deploying at higher Mach numbers. However, these options were not addressed in the present analysis.



**Figure 6: Parachute Deployment MOLA Altitude vs. Landing Ellipse Length for Various EFPA**

## VIII. Performance of Smart Divert for Random Terrain

For missions that have not yet been defined, the exact layout of the terrain is unknown. Consequently, the optimal quantity and arrangement of safe zones are difficult to precisely quantify. As such, a Monte Carlo was performed that included the location of the safe zones as uncertain parameters. In this analysis, random placement of the safe zone sites was statistically performed to model the effect of randomly distributed terrain hazards across the range of actual Mars landing sites of interest. The nominal MSL EFPA of  $-15.7^\circ$  was used, resulting in a parachute deployment MOLA altitude of approximately 2.5 km and landed ellipse length of approximately 35 km. The safe zones were chosen randomly from the target ellipse created around the ballistic impact footprint as shown in Figure 7. It will be shown that locating the safe zones near the ballistic impact footprint accounts for the natural motion of the vehicle after parachute release and reduces the amount of propellant required to perform the divert. The safe zones were assumed to be at  $-7.9$  km MOLA altitude, consistent with the lowest elevations on Mars<sup>1</sup>. This results in a divert initiation altitude of approximately 10.5 km and was chosen to ensure the parachute deployment altitude be sufficiently high to perform large divers across the entire uncertainty ellipse when a small number of random safe zones is modeled. A 2,000 case Monte Carlo was performed for various numbers of safe zone targets, and the resulting PMF distributions is shown in Figure 8. As expected, the required PMF necessary to divert decreases as the number of safe zone locations increases. Additionally, four safe zone sites, randomly placed throughout the ellipse, results in a required PMF less than 0.3 for 97% of the cases analyzed assuming MSL state-of-the-art interplanetary navigation. It is important to note that a tail of the distribution does not exist on the low PMF values. Instead, all distributions converge to 0.22, which represents the case in which the safe zone is located along the

natural motion of the vehicle and requires no additional horizontal divert. This is analogous to the case in Figure 5 for a divert distance of 0 km and an altitude of 11.5 km in which the resulting PMF is approximately 0.22.

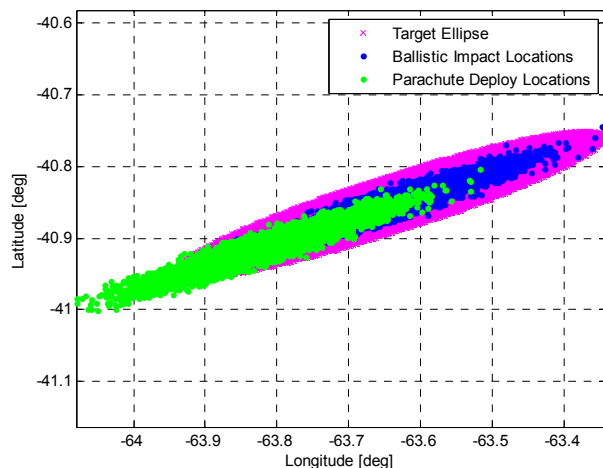


**Figure 7: Target Ellipse Fitted to Ballistic Impact Locations**

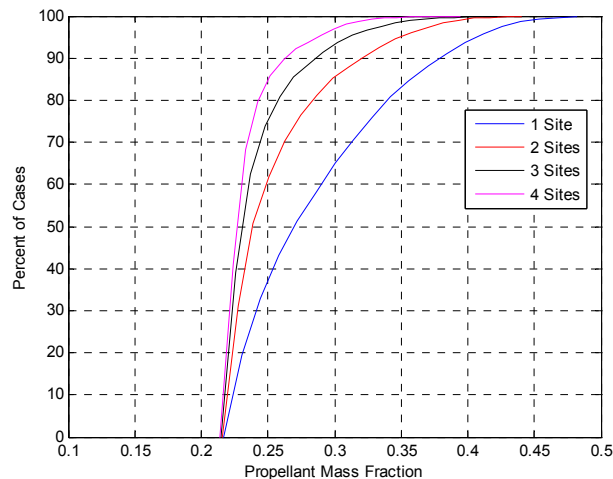


**Figure 8: Cumulative Distribution Function of PMF for Various Numbers of Sites**

### IX. Optimal Landing Site Arrangement

For an actual mission, safe zones will not be randomly placed inside the landed ellipse. Instead, the Mars surface will dictate what is possible and mission designers, after evaluating many options, will have some flexibility in the number and arrangement of the safe zones to meet the mission’s science objectives within an available propellant budget. The optimal arrangement of safe zones can be assessed assuming hazard free terrain in which the location of the optimally arranged safe zones is not constrained. In order to reduce execution time, only 100 dispersed cases were used in the Monte Carlo. The nominal MSL EFPA of  $-15.7^\circ$  was used again, resulting in a landed ellipse length of 35 km. Similar to the random terrain analysis, the potential safe zones were chosen within the target ellipse that was fitted around the ballistic impact footprint to account for the large horizontal velocity at parachute jettison. The full design space of 485 potential safe zones was discretized inside the target ellipse and is shown in Figure 9. The safe zones were assumed to be located at -7.9 km MOLA to ensure each dispersed trajectory had sufficient altitude to divert to each safe zone during this analysis. The optimal arrangement for various numbers of the safe zones was obtained to minimize the maximum required PMF based on the 100 case Monte Carlo. Optimization was performed using a grid search technique. After all 100 case Monte Carlos were performed for each safe zone, the PMF required to divert to each safe zone for all dispersed trajectories was known. This allowed for a straightforward evaluation to determine which combination of safe zones would be optimal, and this method could be repeated regardless of the number of safe zones desired.

The optimal site arrangement for various numbers of safe zones is shown in Figure 10. As expected, the optimal arrangement consisted of divert sites located near the centerline of the target ellipse. As can be seen, one safe zone is optimally placed in the center of the target ellipse, and two safe zones are mirrored about the center of the target ellipse and are along the centerline of the target ellipse. This verifies that biasing the safe zones downrange according to the ballistic impact locations is sufficient for Smart Divert. As the number of safe zones increases, the arrangement of the safe zones deviates slightly from the centerline of the target ellipse. This result is an artifact of the sites becoming biased to the 100 Monte Carlo cases. As more safe zones are added to the optimization, some of the safe zones are placed off the centerline of the target ellipse to reduce the PMF of the worst case dispersed trajectories. In the future, a better sampling of cases from the Monte Carlo that are distributed more evenly throughout the parachute deploy ellipse should be chosen to prevent this bias. The maximum required PMF for the various number of safe zone sites is shown in Table 4. As expected, the maximum required PMF decreases as the number of safe zones increases. At four safe zones, the required PMF approaches the minimum required PMF for the high altitude in which

**Table 4: Maximum Required PMF for Various Number of Safe Zones**

Number of Safe Zones	Maximum Required PMF
1	0.2645
2	0.2308
3	0.2223
4	0.2204

the divert is initiated, consistent with the minimum PMF of 0.22 found for the random site analysis (Figure 8) and the initial sensitivity analysis (Figure 5). It is important to note that only a few safe zones are required due to the small length (35 km) of the landed footprint. For larger landed footprints or low parachute deployment altitudes, more safe zones would be required throughout the ballistic impact ellipse to ensure each dispersed trajectory can feasibly divert to at least one safe zone.

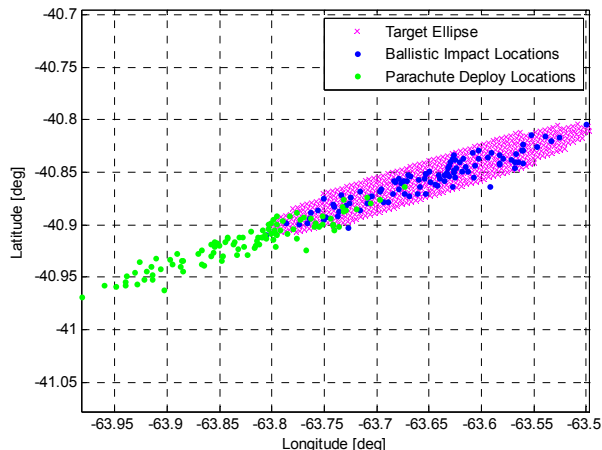


**Figure 9: Potential Smart Divert Sites Fitted Around Parachute Deploy Locations**

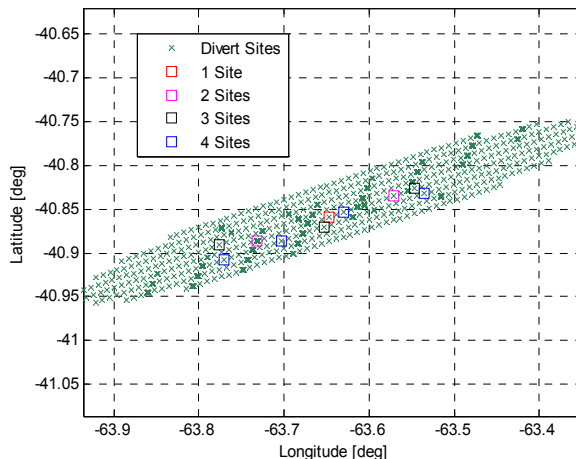


**Figure 10: Divert Site Optimization**

### X. Influence of Entry on Number of Safe Zones

Several key factors drive the landed ellipse size for ballistic entries. As shown in Figure 6, ballistic entries have a dependence between parachute deploy altitude and ellipse length. As the entry flight path angle is shallowed, higher parachute deploy altitudes are achieved at the penalty of larger ellipse lengths. Ellipse length is also a function of interplanetary navigation accuracy. Previous direct entry ballistic missions have had 3-sigma landed ellipse lengths as large as 200-300 km (Mars Pathfinder and Phoenix) and as small as 80 km (MER).

Through use of an onboard hypersonic guidance algorithm, a lifting vehicle, such as the MSL aeroshell, can manipulate the direction of the lift vector to achieve both a higher parachute deploy altitude and a reduced landed footprint length. For MSL, the 3-sigma landed ellipse size has been reduced to approximately 20 km. In addition, pinpoint landing studies have shown that additional precision in the entry phase to reduce the parachute deployment footprint length to approximately 3 km represents a limit in which further improvement does not reduce the overall required propellant mass<sup>5</sup>.

The ability of the vehicle to divert increases as the propellant budget (or PMF) of the vehicle increases. Knowledge of the vehicle PMF could therefore be used with Figure 5 to develop a general guideline for the approximate number of safe zones required as a function of ellipse length. As previously mentioned, an unguided gravity turn requires a PMF of 0.15, and, as a guideline, it is unlikely that mission designers would more than double the PMF for Smart Divert missions. Therefore, PMF values of 0.2 and 0.3 are considered to develop this general guideline. As shown in Figure 5, a PMF of 0.2 results in a divert capability of approximately 5 km; whereas, a PMF of 0.3 results in a divert capability of approximately 10 km.

Assuming hazard free terrain, safe zones would likely be spaced evenly throughout the ellipse to minimize the number of required safe zones. To accommodate the entire ellipse with a minimum number of safe zones, the distance of a safe zone from any dispersed trajectory must not exceed the divert capability of the vehicle. Therefore, as a general guideline, the number of required safe zones would simply be a ratio of the area of the landed ellipse to the area of the divert capability of the vehicle to each safe zone. The required number of safe zones for various landed footprint sizes of interest is shown in Table 5. Based on the Phoenix mission,

**Table 5: Guideline for Required Number of Safe Zones**

Landed Footprint Length [km]	Number of Safe Zones Required (PMF = 0.2)	Number of Safe Zones Required (PMF = 0.3)
200	67	17
80	12	5
20	4	1
3	1	1

the 200-km 3-sigma landed ellipse was assumed to have a major axis to minor axis ratio of approximately 6. However, based on MSL and pinpoint landing studies, the 20-km and 3-km 3-sigma landed ellipse were assumed to be circular. As expected, the number of safe zones required for a Phoenix-like mission is quite large, and the use of entry guidance can be used to significantly reduce the number of required safe zones.

The safe zones were assumed to resemble a single point. Assuming a PMF of 0.2 and corresponding divert capability of 5 km, an example arrangement of these safe zones for the 80 km landing ellipse and the 20 km circular landing footprint is shown in Figure 11 and Figure 12, respectively. The divert capability circles around each safe site represents locations in the landing footprint from which the vehicle could divert to the safe site. Hazardous terrain can exist throughout the divert capability circles since the vehicle is capable of diverting to a safe zone. As can be seen, locations in the landing footprint exist where the vehicle would not have the capability to divert to at least one safe site. If hazardous terrain exists in these regions, then additional safe sites must be added to extend divert coverage over the hazardous terrain. In reality, safe zones will not consist of single points and will encompass a region of hazard-free terrain. The divert capability contours would no longer be circles and would extend a distance away from the safe zone equivalent to the divert capability of the vehicle.

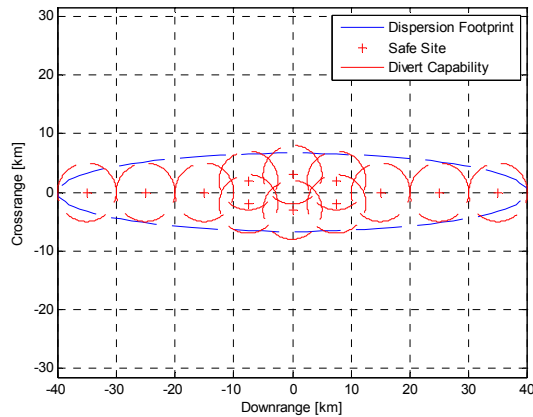


**Figure 11: Safe Site Placement for 80 km Landing Ellipse for 5 km Divert Capability**

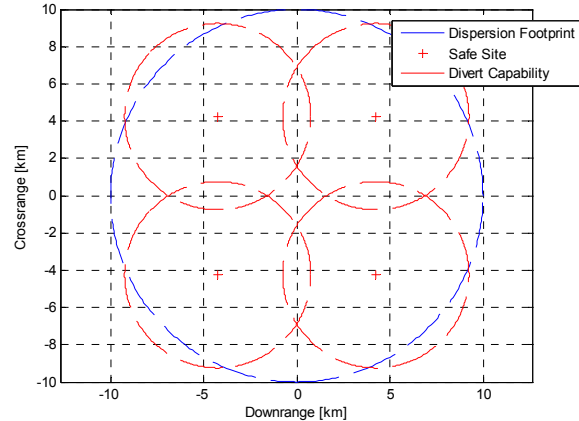


**Figure 12: Safe Site Placement for 20 km Circular Landing Footprint for 5 km Divert Capability**

## XI. Phoenix Example

In order to demonstrate the capability of Smart Divert for a real mission scenario, rock count data for the Phoenix landing region was obtained. A contour of the rock count data may be seen in Figure 13.<sup>8</sup> The red regions correspond to approximately 250 observed rocks per hectare and the dark blue regions correspond to very few observed rocks per hectare. This rock count data was constructed from orbital observations using the High Resolution Imaging Science Experiment (HiRISE) on the Mars Reconnaissance Orbiter (MRO). The resolution of HiRISE allows the identification of rocks 1.5 m

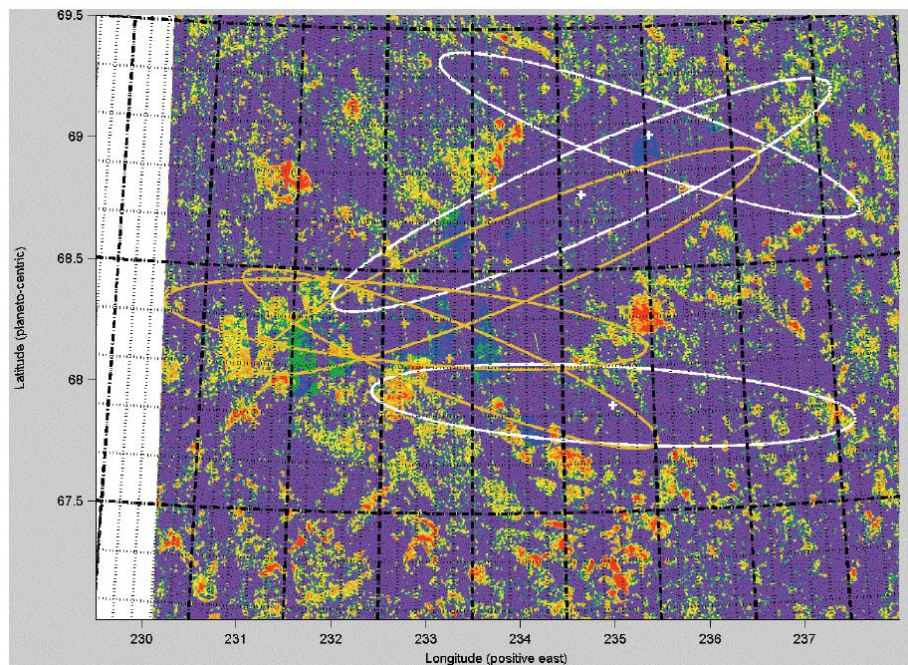


**Figure 13: Phoenix Landing Region Rock Count**

in diameter or larger. These rocks were counted by hand and by using autonomous software. The rock counting is performed by identifying shadows cast by rocks and large changes in albedo caused by dust surrounding rocks. As shown in Figure 13, various options existed to orient the landing ellipse for Phoenix (denoted by the white and gold ellipses). The mission design team’s goal essentially became to place the Phoenix 3-sigma landed ellipse over a region with the fewest rocks to maximize the probability of landing safely. However, given the size of the Phoenix 3-sigma landed footprint, not all regions of the various landing ellipse are rock-free. In fact, certain portions of the ellipses cross regions with high rock counts.

A subset of the Phoenix landing region is shown in Figure 14. This region is 50 km by 20 km. Note that the scaling of colors has changed with the red regions now corresponding to fifty 1.5 m diameter rocks or larger per hectare. This would have been considered an extremely hazardous region to attempt to land the Phoenix spacecraft. In fact, no previous or presently planned lander would be capable of safely targeting a landing in this region. However, blue safe zone regions, denoted by magenta stars, with few rocks can be found embedded within the hazardous red regions. As such, if the Phoenix vehicle had been capable of autonomously diverting to one of these *apriori* identified fuel-optimal safe zones, then the Phoenix ballistic landed ellipse could have been placed over this larger region despite its significant rock abundance. In cases like this, Smart Divert may provide a way to land in these previously unreachable regions.

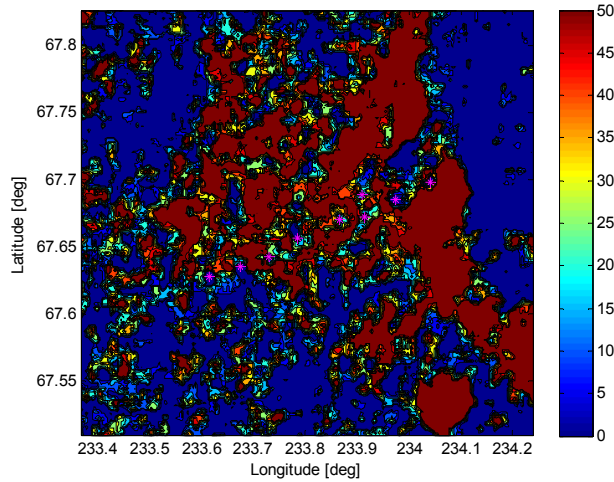


**Figure 14: Subset of Phoenix Landing Site Rock Count Data per Hectare**

As shown in Figure 15, the geometry of the Figure 14 magenta safe zones and the Phoenix landing elevation of -4 km MOLA were preserved and placed downrange of the ballistic parachute deploy footprint resulting from the MSL covariance. This resulted in a parachute deployment altitude of 6.5 km, allowing sufficient timeline for the final EDL events. In this simulation, the parachute is released at Mach 0.8 and the vehicle propulsively diverts to the fuel-optimal safe zone denoted by red squares. The touchdown locations for all the dispersed trajectories are shown as blue dots, and, as can be seen, all dispersed trajectories are capable of reaching a safe zone. The resulting cumulative distribution function of PMF may be seen in Figure 16. For this mission, Smart Divert requires a PMF less than 0.2 for all cases. This PMF is lower than the previously seen cases due to the lower parachute deploy altitude and the large number of safe zones (nine) for the small landed footprint (35 km). Smart Divert is a simple

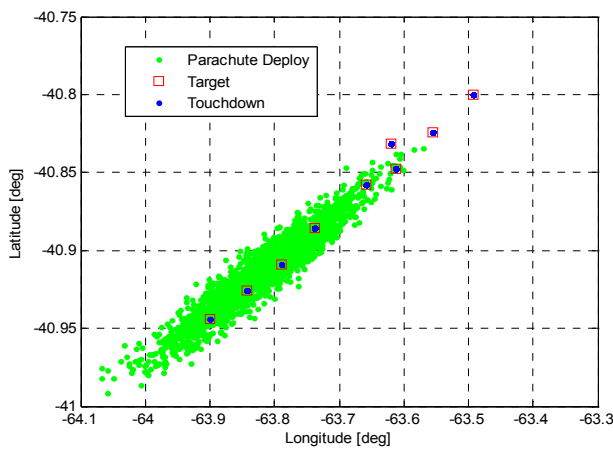


**Figure 15: Snapshots of Various States**

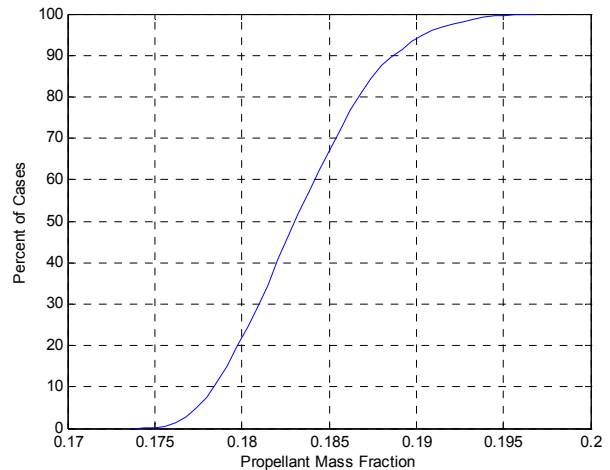


**Figure 16: Cumulative Distribution Function of Propellant Mass Fraction**

EDL architecture capable of safely landing a vehicle in hazardous, scientifically interesting terrain. Again, it is important to note that favorable PMF values were obtained by biasing the safe zones downrange from the parachute deploy ellipse to account for the horizontal velocity at parachute deploy.

## **XII. Conclusion**

Smart Divert is a new, low cost EDL architecture consisting of a ballistic entry, supersonic parachute deployment, and an autonomous landing site selection that may provide a simple approach to safe landing of vehicles in hazardous terrain. An MSL-class vehicle was studied in order to demonstrate the capability of Smart Divert for future large Mars landers. In order to restrict the required PMF to less than 0.3 a maximum divert of 10 km or less should be initiated no lower than 5 km AGL such that sufficient timeline exists for the remaining EDL events.

The elevation of the landing region governs the design of the nominal ballistic entry flight path angle. Shallower entries provide higher supersonic parachute deployment altitudes, allowing diverts to high elevations. However, shallow ballistic entries result in large landing ellipse lengths, requiring more Smart Divert safe zones to maintain reasonable PMF requirements.

The influence of the number of Smart Divert sites was quantified for a random terrain in which the location of the safe zone sites were randomly varied in a Monte Carlo simulation assuming a landed footprint length of 35 km. Four sites randomly placed allowed 97% of the simulations to land safely with a PMF less than 0.3. An example method of optimal landing site arrangement demonstrated that the ballistic impact footprint provides sufficient downrange bias in safe zones to account for the horizontal velocity at supersonic parachute jettison. As expected, the sites were located near the major axis of the target ellipse. A general guideline was developed to determine the number of safe zones required for various 3-sigma landed ellipse sizes assuming hazard-free terrain. A Phoenix-like entry resulting in a landed ellipse length of 200 km would require approximately 17 or more safe zones, depending on the available PMF of the vehicle. The number of safe zones would be reduced to four or less for a 20-km 3-sigma landing ellipse major axis.

An example EDL scenario using rock count data from the Phoenix landing region demonstrated that Smart Divert can provide the capability to safely land entry vehicles in hazardous terrain even when only a small fraction of the terrain is regarded as safe. For the example considered, a minimal PMF (less than 0.2) would have been required to successfully perform the necessary diverts to ensure the Phoenix lander reached the surface safely. This result is even more striking given the fact that, due to landed safety concerns, no previous or presently planned lander have targeted a landing in this region. Hence, Smart Divert could provide the means to send vehicles to hazardous, rock populated landing areas.

Finally, it is important to note that Smart Divert could be performed using existing sensor technology. In order to perform Smart Divert, the vehicle must be aware of its current position and velocity relative to pre-designated target sites during terminal descent. This information can be obtained from a combination of inertial measurement unit (IMU), terminal descent radar, and optical camera data.

## **XIII. Future Work**

The influence of interplanetary navigation must be assessed. This study assumed state-of-the-art navigation quantified in the MSL entry covariance with a resulting 35-km parachute deployment footprint. For larger parachute deployment footprints, the Smart Divert concept is likely to provide additional landing safety and mission design flexibility. An assessment of methods to identify the fuel-optimal divert site should also be performed. This analysis required an onboard evaluation of all sites by propagating simple equations of motion using the D'Souza guidance to identify the fuel-optimal safe zone. Due to the simplicity of ballistic entries, measurable entry characteristics such as peak deceleration load could potentially be used to infer the location of the vehicle inside the landed ellipse and thus can be used to select the fuel-optimal divert site without requiring the onboard propagation of equations of motion. It is possible that these pre-selected sites along with measurable entry characteristics could be evaluated on the ground prior to entry, eliminating the need for real-time, autonomous site selection.

## **References**

<sup>1</sup> Braun, R.D. and Manning, R.M., "Mars Exploration Entry, Descent, and Landing Challenges," *Journal of Spacecraft and Rockets*, Vol. 44, No. 2, pp. 310-323, 2007.

<sup>2</sup> Mendeck, G.F. and Carman, G.L., "Guidance Design for Mars Smart Landers Using The Entry Terminal Point Controller," AIAA-2002-4502, AIAA Atmospheric Flight Mechanics Conference and Exhibit, Monterey, California, 5-8 August 2002.

<sup>3</sup> Cheng, Y. Johnson, A. and Matthies, L. "MER-DIMES: A Planetary Landing Application of Computer Vision," IEEE Computer Society Conference on Computer Vision and Pattern Recognition, 2005.

<sup>4</sup> Striepe, S., Way D., Dwyer, A., "Mars Science Laboratory Simulations for Entry, Descent, and Landing," Journal of Spacecraft and Rockets, Vol. 43, No.2, 2006, pp. 311-323.

<sup>5</sup> Steinfeldt, B.A., Grant, M.J., Matz, D.M., and Braun, R.D., "Guidance, Navigation, and Control Technology System Trades for Mars Pinpoint Landing," AIAA-2008-6216, AIAA Atmospheric Flight Mechanics Conference, Honolulu, Hawaii, 18-21 August 2008.

<sup>6</sup> D'Souza, C., "An Optimal Guidance Law for Planetary Landing," AIAA 97-3709, AIAA Guidance, Navigation, and Control Conference, New Orleans, Louisiana, 11-13 August 1997.

<sup>7</sup> Wolf, A., Tooley, J., Ploen, S., Gromov, K., Ivanov, M., and Acikmese, B., "Performance Trades for Mars Pinpoint Landing," IEEE Aerospace Conference, Paper 1661, Big Sky, Montana, March 2006.

<sup>8</sup> Bonfiglio, E., Adams, D., Craig, L., et al., "Landing Site Dispersion Analysis and Statistical Assessment for the Mars Phoenix Lander," AIAA 2008-7348, AIAA/AAS Astrodynamics Specialist Conference and Exhibit, Honolulu, Hawaii, 18-21 August 2008.